

Review

# The Use of CBCT in Evaluating the Health and Pathology of the Maxillary Sinus

Andy Wai Kan Yeung <sup>1</sup>, Kuo Feng Hung <sup>2</sup>, Dion Tik Shun Li <sup>2</sup> and Yiu Yan Leung <sup>2,\*</sup>

<sup>1</sup> Oral and Maxillofacial Radiology, Applied Oral Sciences and Community Dental Care, Faculty of Dentistry, The University of Hong Kong, Hong Kong SAR, China

<sup>2</sup> Oral and Maxillofacial Surgery, Faculty of Dentistry, The University of Hong Kong, Hong Kong SAR, China

\* Correspondence: mikeyyleung@hku.hk

**Abstract:** The use of cone-beam computed tomography (CBCT) has been increasing in dental practice. This narrative review summarized the relevance and utilizations of CBCT to visualize anatomical structures of the maxillary sinus and common pathologies found in the maxillary sinus. The detection/visualization rate, the location and the morphometric characteristics were described. For sinus anatomy, the reviewed features included the posterior superior alveolar artery, sinus pneumatization, sinus hypoplasia, sinus septa, and primary and accessory sinus ostia. For pathology, the following items were reviewed: membrane thickening associated with periapical lesions/periodontal lesions, mucous retention cyst, and antrolith. The visualization and assessment of the maxillary sinus is very important prior to procedures that take place in close proximity with the sinus floor, such as tooth extraction, implant insertion, and sinus floor elevation. Some sinus pathologies may be associated with odontogenic lesions, such as periapical diseases and periodontal bone loss.

**Keywords:** cone beam computed tomography; CBCT; maxillary sinus; Schneiderian membrane; health; pathology; sinus floor elevation



**Citation:** Yeung, A.W.K.; Hung, K.F.; Li, D.T.S.; Leung, Y.Y. The Use of CBCT in Evaluating the Health and Pathology of the Maxillary Sinus. *Diagnostics* **2022**, *12*, 2819. <https://doi.org/10.3390/diagnostics12112819>

Academic Editor: Elina A. Genina

Received: 26 October 2022

Accepted: 15 November 2022

Published: 16 November 2022

**Publisher's Note:** MDPI stays neutral with regard to jurisdictional claims in published maps and institutional affiliations.



**Copyright:** © 2022 by the authors. Licensee MDPI, Basel, Switzerland. This article is an open access article distributed under the terms and conditions of the Creative Commons Attribution (CC BY) license (<https://creativecommons.org/licenses/by/4.0/>).

## 1. Introduction

The maxillary sinuses are a pair of large air-filled cavities located superior to the posterior part of the dentoalveolar region of the maxilla. The maxillary sinus has the shape of a pyramid and is the largest among the four paranasal sinuses. It drains into the middle meatus of the nasal cavity. It has three recesses, the alveolar process, the zygomatic recess, and the infraorbital recess. Due to the proximity of the sinus floor with the alveolar ridge, the maxillary sinus is of high relevance to multiple dental procedures, ranging from tooth extraction to implant insertion. When the sinus condition should be considered during diagnosis and treatment planning, the cone beam computed tomography (CBCT) is the optimal choice among the common imaging modalities, as it allows a 3D visualization of the structure either entirely or partially, and without the limitation of superimposition with other structures as with 2D imaging. It was reported that 10–14% of the population in Europe and the United States suffered from chronic sinusitis, which could be rhinosinusal or odontogenic [1]. Subsequently, pathologies of the paranasal sinuses were common incidental findings from CBCT imaging [2]. For example, panoramic radiography could not accurately demonstrate root proximity with the sinus floor when there was root contact with the sinus floor on the buccal or palatal side [3]. In these circumstances, panoramic radiography tended to overestimate the extent of root protrusion into the sinus [4], and could make the root appear to be in the sinus [5]. Similarly, panoramic radiography showed inferior performance in detecting sinus membrane thickening [6], sinus septum [7], or oroantral communication after tooth extraction [8]. On the other hand, anatomical variations of the maxillary sinus could sometimes “false positively” presented as apparent odontogenic lesions such as radicular cysts associated with maxillary teeth on a panoramic radiograph, which required further evaluation by CBCT [9].

Dental CBCT machines were developed and commercialized near the end of the 1990s and since then they have been heavily used in dental implant research to assess the condition of the maxillary sinus [10,11]. In fact, the European Academy of Dentomaxillofacial Radiology (EADMFR) advocated a minimum level and core content for training dentists who were involved in CBCT imaging and interpretation for general dentists [12]. In Level 1, a general dentist should be able to use CBCT machines, analyse normal anatomical structures of the teeth, jaws and facial skeleton in CBCT images, and recognize both anatomy and disease of the teeth and supporting structures in CBCT images [12]. In Level 2, a general dentist should be able to differentiate between findings indicating normal anatomical structures from those of diseased teeth, jaws and facial skeleton [12]. Therefore, the correct interpretation of the status of the maxillary sinus is one important aspect in reading CBCT images, as the sinus is frequently in close proximity of the root apices of the maxillary posterior teeth.

In clinical practice, one of the most frequent indications for dental CBCT imaging was the dimensional and health assessment of the alveolar ridge and maxillary sinus for implant planning and sinus lift procedures [13], including the assessment of the bone graft volume required [14]. Indeed, several authorities have advocated the use of CBCT for pre-operative evaluation of the implant planning sites [15–17]. Besides implant planning, evaluating the health status of the maxillary sinuses during the diagnostic and treatment planning procedures has also been suggested in other scenarios, such as orthodontics [18], pre-operative assessment of teeth undergoing apical surgery [19], and evaluation of cystic and neoplastic lesions in the maxillary region especially if the posterior region was involved [20].

As mentioned above, a CBCT scan produces a 3D image volume, and hence its radiation dose is usually higher than a plain radiograph such as a panoramic or a periapical radiograph. Some clinicians may thus minimize the use of CBCT and subsequently be unfamiliar with the advantages of this modality over plain radiography in evaluating the maxillary sinus. With the versatility of a CBCT machine, multiple parameters ranging from the spatial resolution, peak voltage to the number of projections can be adjusted to optimize the radiation dose emitted, such that the principle of “as low as reasonably achievable” (ALARA) has gone through a long history of evolution [21], with some expert opinions that advocated to rename it to “as low as diagnostically acceptable” (ALADA) [22] and, more recently, “as low as diagnostically acceptable being indication-oriented and patient-specific” (ALADAIP) [23]. One quality assurance measure to optimize the radiation dose is to establish institutional or national dose reference levels (DRLs) for each indication of CBCT examinations. For instance, it was suggested that the DRL for a CBCT examination to evaluate maxillary sinus pathology could be in the range of 520–1150 mGy × cm<sup>2</sup> [24]. Another measure is to enhance user training to minimize the chance of a retake due to inadequate diagnostic value of the original scan. It was recently reported that CBCT retake rate was approximately 2.8% across studies [25], and that inadequate visualization of the maxillary sinus was one of the commonest reasons for a retake [26].

The anatomical variants of the maxillary sinus are mainly sinus septations, presence of accessory sinus ostium, and sinus hypoplasia, among the others [27]. Meanwhile, its pathologies can generally be classified into inflammatory, iatrogenic, traumatic, neoplastic, odontogenic, congenital and bone-related [28]. This narrative review aimed to provide an overview of the findings from published CBCT studies that evaluated the anatomy and pathology of the maxillary sinus.

## 2. Anatomy

### 2.1. Posterior Superior Alveolar Artery (PSAA) and Lateral Wall Thickness

The PSAA is a branch of the maxillary artery that runs along and supplies the lateral wall of the maxillary sinus and the overlying Schneiderian membrane (Figure 1). It should be carefully considered during sinus grafting procedures as there may be a potential risk of profound bleeding [29]. Severe bleeding after damaging PSAA during sinus floor elevation with transcrestal technique has been documented [30]. The detection/visualization rate of

PSAA on CBCT scans ranged from around 48.6 to 91.6% [31–36]. PSAA could be mostly found below the sinus membrane (13–63.8%) or intraosseous (28.5–71.1%), but less frequent at the outer cortex of the lateral wall of the sinus (5.2–9.9%) [31–36]. The apparent absence of PSAA in some CBCT scans could be due to its small size or lying immediately on either side of the lateral wall of the sinus without forming bone indentation [36]. For a meta-analysis on the prevalence of PSAA in a pooled collection of CBCT and CT studies, readers should refer to [37].

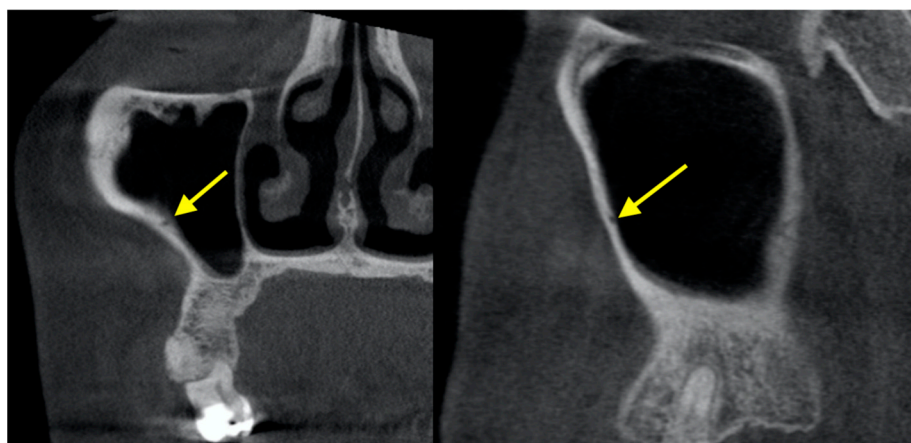


**Figure 1.** Posterior superior alveolar artery shown in CBCT.

Meanwhile, the lateral wall thickness of the maxillary sinus might be critically assessed by CBCT imaging during lateral sinus elevation procedures. A retrospective study of 209 patients with CBCT scans found that the overall mean lateral wall thickness was  $1.6 \pm 0.8$  mm at both 4 mm and 6 mm apical (superior) to the sinus floor [38]. However, cases with membrane perforation during operation had a mean lateral wall thickness of  $2.4 \pm 0.6$  mm at both 4 mm and 6 mm apical to the sinus floor, compared to  $1.2 \pm 0.4$  mm for the non-perforation cases [38]. The lateral wall of the maxillary sinus was also found to be thicker in partial edentulism cases ( $1.3 \pm 0.3$  mm) compared to complete edentulism cases ( $1.0 \pm 0.3$  mm), and positively correlated with residual ridge height [39]. Considering the mesiodistal direction, the lateral wall thickness at 30–40 mm inferior to the orbital floor showed a gradual reduction from the canine region towards the second molar region [40]. There was a positive correlation between the diameter of PSAA and the thickness of the lateral wall of the maxillary sinus [41].

## 2.2. Pneumatization

Maxillary sinus pneumatization does not seem to have a precise definition. In general, it refers to the maxillary sinus extension into a particular anatomical structure, such as the alveolar ridge, maxillary tuberosity, and palate [42]. For instance, alveolar pneumatization was considered present if the maxillary sinus floor was coronal to the apex of one of the roots of the posterior teeth [43]. Its overall prevalence from CBCT studies ranged from 23.5% to 83.2% [42,43]. It was more common among patients aged between 18 and 34 years (66.4%), followed by those aged between 35–59 years (36.8%) and those aged 60 years or above (22.3%) [44]. It was believed that the alveolar pneumatization was the most common variant, involved in as many as 100% of patients with sinus pneumatization, followed by the palate/palatal process (23.6%), maxillary tuberosity (22%), and anterior region (5.2%) [42]. Alveolar pneumatization tended to be most severe between the first and second molars (13.8–14.0 mm), followed by between the second and third molars (13.22 mm) and between the second premolar and first molar (9.1–9.2 mm) [45]. Similarly, localized sinus pneumatization following tooth loss was more likely to occur at the first molar (37.9%), compared to the second molar (12.1%) [43]. After minimally traumatic molar extraction, alveolar ridge preservation with synthetic nanohydroxyapatite was found to associate with

0.7 mm sinus pneumatization, slightly smaller than the 1.0 mm from unassisted socket healing [46]. The difference was statistically insignificant [46]. For palatal pneumatization, most of them (>99%) did not extend medially to exceed one-half of the width of the nasal floor [47].

### 2.3. Hypoplasia

In contrast to sinus pneumatization, sinus hypoplasia leads to reduced sinus cavity volume. At first glance, this seems to be a favourable condition given the ample distance between the dentoalveolar region and the sinus floor. However, the presence of sinus hypoplasia in CBCT images was found to significantly increase the prevalence of sinus mucosal thickening and blocked ostium (68.3% vs. 25.6%) [48]. The prevalence of sinus hypoplasia was reported to be around 0.2–50% [42,48,49]. Most of the cases belonged to Type I (69.5%; mild hypoplasia, normal uncinat process, and patent infundibular tract) or Type II (25.6%; moderate hypoplasia, hypoplastic uncinat process, and ill-defined or absent infundibular tract). Type III accounted for a minority (4.9%; severe sinus hypoplasia and absence of uncinat process) [48]. In rare circumstances, aplasia might be found from CBCT imaging as an incidental finding [50]. Apart from sinus health, sinus hypoplasia did not seem to affect the health or functions of dentoalveolar structures, such as canting of the maxillary occlusal plane, open bite, or mandibular asymmetry [51].

### 2.4. Sinus Augmentation

In implant cases where the severely resorbed alveolar bone ridge was unable to accommodate an implant, sinus augmentation procedure should be performed to increase the amount of bone inferior to the maxillary sinus floor. Recent CBCT studies found that such bone graft volume decreased by an average of 25% after 4.7–6 months of healing [52,53]. From 6 months after grafting until 3 years after grafting, the graft volume could be reduced by an average of 27.4–39.3% [53,54]. However, one CBCT study found no such significant reduction in the graft volume 4–7 months after the surgery [55]. Apart from bone volume, the bone mineral density is also an important factor for successful implantation. The gray level measured at the implant sites in CBCT images was found to have a good correlation to the actual mineralized material content computed by microradiography of the bone core biopsies taken at the implant sites [56]. Additionally, the gray level of sites grafted with bovine bone materials remained stable at 4–7 months of follow-up [55].

### 2.5. Septa

The presence of sinus septa at the sinus floor and lateral wall of the sinus may hinder sinus lift procedures (Figure 2). The prevalence of sinus septa was around 27.1–59.7% [42,57–60]. Septa could be orientated in a coronal direction (61.8–79.2%), axial direction (4.9–22.3%) or sagittal directions (3.6–24.5%) [57–59,61]. As many as 4 septa within one sinus have been reported [57,58]. In the caudocranial direction, septa was most prevalent in the sinus floor (58.6%), followed by roof (33.1%), anterior wall (6.7%), posterior wall (1.2%), and lateral/medial wall (0.4%) [57]. In the anteroposterior direction, septa was most prevalent in the region of the 1st and 2nd molars (37.2–69.1%), followed by the region of the third molar (18.6–33.0%) and the region of the canines and premolars (12.2–29.8%) [59,60].

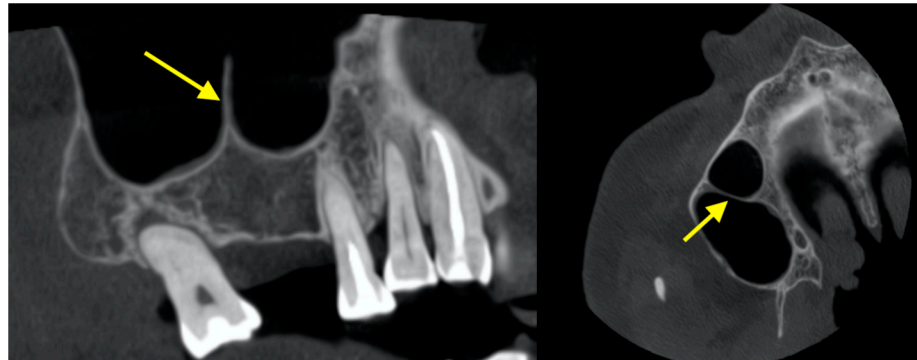


**Figure 2.** Nasal septum on the sinus floor.

### 2.6. Primary and Accessory Ostia

The sinus cavity is drained into the nasal cavity by mucociliary clearance system through the (primary) sinus ostium (Figure 3). Drainage is severed if the ostium is blocked. Ostium patency in CBCT images was found to be around 87.0–94.0% [62–64]. It is located above the attachment of the inferior turbinate, and most of the time it was located in the middle third (76.1%) of the turbinate or the anterior third (23.7%) [64]. Most sinus ostia were reported to be slit shaped (71.1%), followed by ovoid (22.3%) and round (6.6%) [64]. Obstruction was significantly more likely to occur if the sinus had sinusitis or >10 mm membrane thickening [62,64]. Immediately after sinus floor elevation, it was estimated that obstruction occurred for up to 30% of the sinus ostia, which were mostly resolved at 7.5-month follow-up [63].

Meanwhile, the prevalence of accessory ostium was 35.5–56.7% [64–67]. Contrast to primary ostium, the accessory ostium was usually ovaloid (48.4%) or round (39.0%) instead of slit shaped (12.6%) [65]. The accessory ostium, if present, was on average  $19.9 \pm 1.7$  mm from the most inferior point of the sinus floor [67]. The presence of sinusitis or mucosal thickening and accessory ostium were associated [66,67].

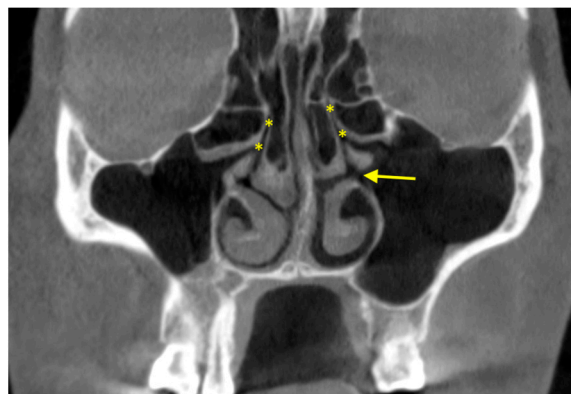


**Figure 3.** Primary ostium (asterisk) in both maxillary sinuses and accessory ostium (arrow) in the left maxillary sinus.

## 3. Pathology

### 3.1. Membrane Thickening Associated with Periapical Lesions

Sinus membrane thickening associated with an endodontically involved tooth was common (Figure 4). It has been reported by numerous studies [68–71]. In one study, the sinus membrane was, on average, 2.56–2.74 mm thick in cases with associated teeth having apical pathology, which was significantly thicker than the healthy controls (1.18–1.21 mm) [70]. In another study, the prevalence of membrane thickening was reported to be 41.5% for patients with no associated teeth with apical periodontitis, but increased to around 70% for those with visible small changes in bone structure to a well-defined radiolucent periapical area,

and further increased to 100% for those with severe apical periodontitis [68]. Results from a more recent study were consistent to prior findings, in that sinuses with >2 mm membrane thickening were more likely to have associated teeth with periapical lesions (53.6% versus 42.1%) [69]. The chance of having membrane thickening when there was associated periapical lesions was estimated to be as high as thrice than when there was no periapical lesion [71]. The periapical lesion did not necessarily have to be in contact or enter the sinus floor to elicit sinus membrane thickening [68]. The number of associated root canal treatments also did not influence the degree of thickening [69].

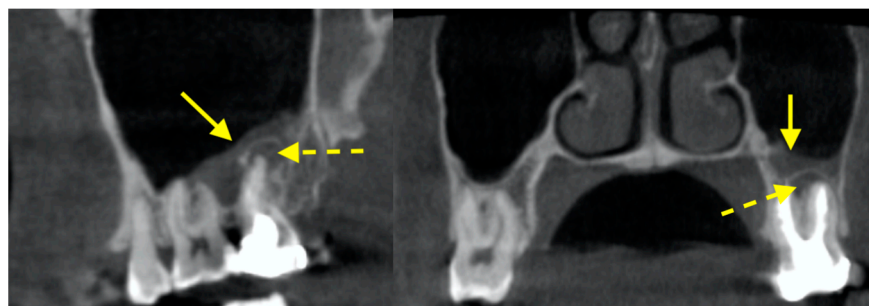


**Figure 4.** Sinus membrane thickening (solid arrow) in the left maxillary sinus associated with a periapical lesion (dotted arrow).

### 3.2. Membrane Thickening Associated with Periodontal Lesions

Similar to periapical lesions, it seemed that membrane thickening was more prevalent when the associated teeth has more severe periodontal bone loss. The chance of membrane thickening for those with severe periodontal bone loss was 4.6 times than those with mild bone loss [72]. Those with class II or class III furcation lesions were 1.6 and 3.5 times, respectively, more likely to have membrane thickening than those without furcation involvement [72]. The presence of vertical intrabony pockets also led to membrane thickening being 2.4–5.6 times more likely than without such pockets [72]. The extraction of the periodontally involved tooth would lead to the complete resolution of the membrane thickening at 4 months [73]. For a comprehensive review on the effect of periapical and periodontal pathologies on membrane thickening, readers can refer to [74].

### 3.3. Mucous Retention Cyst (MRC)

MRCs are commonly found in the maxillary sinus (Figure 5). MRCs were found in 10.1–28.6% of the maxillary sinus [28,75–77]. Up to four MRCs were reported within a single sinus [75,77]. MRCs were more commonly located at the sinus walls (19.9–53.6%) and the floor (28.6–76.7%) instead of the roof (3.4–17.9%) [75,77]. The average size of an MRC was reported to be  $551 \pm 1368 \text{ mm}^3$  with a diameter of  $9.6 \pm 5.4 \text{ mm}$  [76]. The presence of MRCs on the sinus floor was more likely if there were teeth with periapical lesions, were endodontically treated, or with severe bone loss [76,77].



**Figure 5.** Mucous retention cyst in the left maxillary sinus.

### 3.4. Antrolith

Antrolith is a calcified mass in the maxillary sinus (Figure 6). Antroliths were found in 0.6–8.4% of maxillary sinuses [42,78,79]. They could be punctate (14.3–53.1%), linear (31.4–34.3%), or amorphous (15.5–22.9%) [78,80]. Most of them were located at the molar region (95.0%) rather than the premolar region (5.0%), and located in the sinus floor (62.9–77.5%) [79,80]. The size of an antrolith was found to be between 1–91 mm<sup>2</sup>, as measured by the maximum cross-sectional area computed from the coronal slices [78]. Another study reported the mean length was  $5.6 \pm 4.4$  mm, width was  $4.1 \pm 2.9$  mm, and height was  $3.5 \pm 2.1$  mm [79]. Intuitively, the presence of antroliths might seem to pose an increased risk of membrane perforation following implant insertion with simultaneous sinus floor elevation, but study results did not find such increased risk [81].

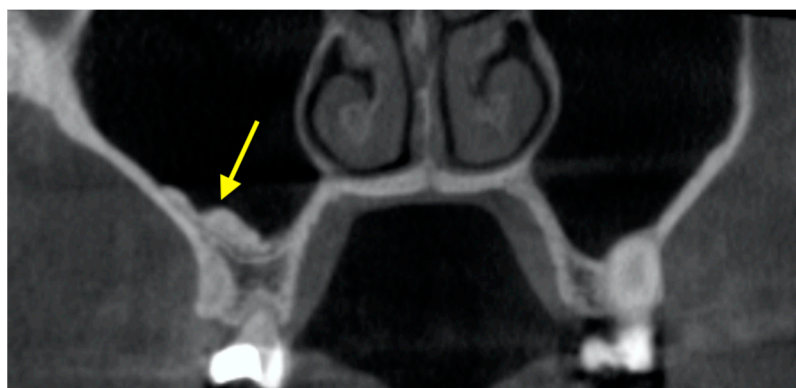


**Figure 6.** Antrolith found on the sinus floor of the right maxillary sinus.

### 3.5. Foreign Bodies

Due to the proximity of the maxillary sinus floor with the dentoalveolar region, iatrogenic introduction of foreign bodies into the sinus can sometimes occur. The foreign bodies can be localized with the aid of CBCT imaging. For example, one study reported 27 patients with foreign bodies introduced into their maxillary sinus, including tooth fragments, complete teeth, dental implants, dental impression material, root filling material, and dental bur [82]. Ample root filling material could be pushed into the maxillary sinus through a perforated root during root canal treatment [83]. Meanwhile, it was found that most of the cases with dental implants introduced into the sinus did not receive a presurgical CBCT exam even in the presence of a severely atrophic edentulous ridge [84]. One uncommon foreign body was a metallic hand sewing needle inserted by a patient into a cavitated tooth to remove trapped food debris, which subsequently disappeared and found to be pushed into the maxillary sinus as confirmed by CBCT [85]. Orthodontic mini-screws might also intrude into the sinus particularly if the sinus floor is <6.0 mm to the alveolar ridge crest [86].

## 4. Artificial Intelligence in Sinus Diagnosis

Nowadays, there are many research works on artificial intelligence including machine learning that can help clinicians detect abnormal findings in the maxillary sinus from CBCT images [87]. To begin with, convolutional neural network (CNN) could be used to automatically segment the maxillary sinus into the bone, air and lesion [88,89], such as MRC [90] or even complete opacification [91]. CNN could also be used to classify if a maxillary sinus was healthy or with sinusitis [92], and to detect the location of the maxillary sinus floor and automatically measure the associated alveolar ridge height for implant planning [93]. In addition, maxillary sinus features, such as sinus volume or linear measurements, were proven to be useful in dental age assessment and sex identification based on CBCT images [94,95]. Meanwhile, CBCT image filter driven by artificial intelligence has been developed to enhance the visualization of the maxillary sinus anatomy for

various diagnostic purposes, such as to evaluate sinus membrane thickening associated with periapical lesions [96].

## 5. Conclusions

The use of CBCT is becoming more and more common in dental practice. The maxillary sinuses can be visualized by CBCT in a medium-to-large field-of-view volume that covers the maxillofacial region. The visualization and assessment of the maxillary sinus is very important prior to procedures that take place in close proximity with the sinus floor, such as tooth extraction, implant insertion, and sinus floor elevation. Some sinus pathologies may be associated with odontogenic lesions, such as periapical diseases and periodontal bone loss. The maxillary sinus may also involve other pathologies, such as fungal infections, allergic pathologies, benign and malignant lesions, and trauma. Clinicians should be familiar with the common anatomical features and sinus pathologies, to facilitate better diagnosis and treatment planning, and promptly refer patients to the oral and maxillofacial surgeons to follow up if needed. This review briefly covered the common and clinically relevant anatomical and pathological features concerning the maxillary sinus. It was intended to increase the awareness of the clinicians about the relevance of sinus health and pathology to clinical dentistry. To recap, the following anatomical features were reviewed: PSAA and lateral wall thickness, sinus pneumatization, sinus hypoplasia, sinus augmentation, sinus septa, and primary and accessory ostia. The following pathological features were reviewed: sinus membrane thickening associated with periapical and periodontal lesions, MRC, antrolith, and foreign bodies. The latest development in artificial intelligence in sinus diagnosis was also covered. Certainly, the features covered were not exhaustive, and readers should refer to specialized oral and maxillofacial radiology textbooks for a comprehensive description of all relevant features and proper image interpretation regarding the maxillary sinus.

**Author Contributions:** A.W.K.Y.; writing—original draft preparation, K.F.H., D.T.S.L. and Y.Y.L.; writing—review and editing. All authors have read and agreed to the published version of the manuscript.

**Funding:** This research received no external funding.

**Institutional Review Board Statement:** Not applicable.

**Informed Consent Statement:** Not applicable.

**Data Availability Statement:** Not applicable.

**Conflicts of Interest:** The authors declare no conflict of interest.

## References

1. Martu, C.; Martu, M.-A.; Maftai, G.-A.; Diaconu-Popa, D.A.; Radulescu, L. Odontogenic Sinusitis: From Diagnosis to Treatment Possibilities—A Narrative Review of Recent Data. *Diagnostics* **2022**, *12*, 1600. [[CrossRef](#)] [[PubMed](#)]
2. Braun, M.J.; Rauneker, T.; Dreyhaupt, J.; Hoffmann, T.K.; Luthardt, R.G.; Schmitz, B.; Dammann, F.; Beer, M. Dental and Maxillofacial Cone Beam CT—High Number of Incidental Findings and Their Impact on Follow-Up and Therapy Management. *Diagnostics* **2022**, *12*, 1036. [[CrossRef](#)] [[PubMed](#)]
3. Lopes, L.J.; Gamba, T.O.; Bertinato, J.V.; Freitas, D.Q. Comparison of panoramic radiography and CBCT to identify maxillary posterior roots invading the maxillary sinus. *Dentomaxillofac. Radiol.* **2016**, *45*, 20160043. [[CrossRef](#)] [[PubMed](#)]
4. Sun, W.; Xia, K.; Tang, L.; Liu, C.; Zou, L.; Liu, J. Accuracy of panoramic radiography in diagnosing maxillary sinus-root relationship: A systematic review and meta-analysis. *Angle Orthod.* **2018**, *88*, 819–829. [[CrossRef](#)]
5. Kirkham-Ali, K.; La, M.; Sher, J.; Sholapurkar, A. Comparison of cone-beam computed tomography and panoramic imaging in assessing the relationship between posterior maxillary tooth roots and the maxillary sinus: A systematic review. *J. Investig. Clin. Dent.* **2019**, *10*, e12402. [[CrossRef](#)]
6. Constantine, S.; Clark, B.; Kiermeier, A.; Anderson, P. Panoramic radiography is of limited value in the evaluation of maxillary sinus disease. *Oral Surg. Oral Med. Oral Pathol. Oral Radiol.* **2019**, *127*, 237–246. [[CrossRef](#)]
7. Lang, A.; Schulze, R. Detection accuracy of maxillary sinus floor septa in panoramic radiographs using CBCT as gold standard: A multi-observer receiver operating characteristic (ROC) study. *Clin. Oral Investig.* **2019**, *23*, 99–105. [[CrossRef](#)]

8. Vollmer, A.; Saravi, B.; Vollmer, M.; Lang, G.M.; Straub, A.; Brands, R.C.; Kübler, A.; Gubik, S.; Hartmann, S. Artificial Intelligence-Based Prediction of Oroantral Communication after Tooth Extraction Utilizing Preoperative Panoramic Radiography. *Diagnostics* **2022**, *12*, 1406. [[CrossRef](#)]
9. Sekerci, A.E.; Sisman, Y.; Etoz, M.; Bulut, D.G. Aberrant anatomical variation of maxillary sinus mimicking periapical cyst: A report of two cases and role of CBCT in diagnosis. *Case Rep. Dent.* **2013**, *2013*, 757645. [[CrossRef](#)]
10. Yeung, A.W.K. Seminal Works and Historical Roots of Dental Implant Research with the Use of CBCT. *Int. J. Oral Maxillofac. Implant.* **2021**, *36*, 731–736. [[CrossRef](#)]
11. Huang, X.; Bai, J.; Liu, X.; Meng, Z.; Shang, Y.; Jiao, T.; Chen, G.; Deng, J. Scientometric analysis of dental implant research over the past 10 years and future research trends. *BioMed Res. Int.* **2021**, *2021*, 6634055. [[CrossRef](#)] [[PubMed](#)]
12. Brown, J.; Jacobs, R.; Levring Jäghagen, E.; Lindh, C.; Baksi, G.; Schulze, D.; Schulze, R. Basic training requirements for the use of dental CBCT by dentists: A position paper prepared by the European Academy of DentoMaxilloFacial Radiology. *Dentomaxillofac. Radiol.* **2014**, *43*, 20130291. [[CrossRef](#)] [[PubMed](#)]
13. Vogiatzi, T.; Kloukos, D.; Scarfe, W.C.; Bornstein, M.M. Incidence of anatomical variations and disease of the maxillary sinuses as identified by cone beam computed tomography: A systematic review. *Int. J. Oral Maxillofac. Implant.* **2014**, *29*, 1301–1314. [[CrossRef](#)] [[PubMed](#)]
14. Hung, K.F.; Hui, L.L.; Leung, Y.Y. Patient-specific estimation of the bone graft volume needed for maxillary sinus floor elevation: A radiographic study using cone-beam computed tomography. *Clin. Oral Investig.* **2022**, *26*, 3875–3884. [[CrossRef](#)]
15. Benavides, E.; Rios, H.F.; Ganz, S.D.; An, C.-H.; Resnik, R.; Reardon, G.T.; Feldman, S.J.; Mah, J.K.; Hatcher, D.; Kim, M.-J. Use of cone beam computed tomography in implant dentistry: The International Congress of Oral Implantologists consensus report. *Implant Dent.* **2012**, *21*, 78–86. [[CrossRef](#)]
16. Bornstein, M.M.; Scarfe, W.C.; Vaughn, V.M.; Jacobs, R. Cone beam computed tomography in implant dentistry: A systematic review focusing on guidelines, indications, and radiation dose risks. *Int. J. Oral Maxillofac. Implant.* **2014**, *29*, 55–77. [[CrossRef](#)]
17. Harris, D.; Horner, K.; Gröndahl, K.; Jacobs, R.; Helmrot, E.; Benic, G.I.; Bornstein, M.M.; Dawood, A.; Quirynen, M. EAO guidelines for the use of diagnostic imaging in implant dentistry 2011. A consensus workshop organized by the European Association for Osseointegration at the Medical University of Warsaw. *Clin. Oral Implant. Res.* **2012**, *23*, 1243–1253. [[CrossRef](#)]
18. Kusnoto, B.; Kaur, P.; Salem, A.; Zhang, Z.; Galang-Boquiren, M.T.; Viana, G.; Evans, C.A.; Manasse, R.; Monahan, R.; BeGole, E. Implementation of ultra-low-dose CBCT for routine 2D orthodontic diagnostic radiographs: Cephalometric landmark identification and image quality assessment. *Semin. Orthod.* **2015**, *21*, 233–247. [[CrossRef](#)]
19. Rigolone, M.; Pasqualini, D.; Bianchi, L.; Berutti, E.; Bianchi, S.D. Vestibular surgical access to the palatine root of the superior first molar: “low-dose cone-beam” CT analysis of the pathway and its anatomic variations. *J. Endod.* **2003**, *29*, 773–775. [[CrossRef](#)]
20. Chindasombatjaroen, J.; Poomsawat, S.; Klongnoi, B. Calcifying cystic odontogenic tumor associated with other lesions: Case report with cone-beam computed tomography findings. *Oral Surg. Oral Med. Oral Pathol. Oral Radiol.* **2012**, *113*, 414–420. [[CrossRef](#)]
21. Yeung, A.W.K. The “As Low As Reasonably Achievable” (ALARA) principle: A brief historical overview and a bibliometric analysis of the most cited publications. *Radioprotection* **2019**, *54*, 103–109. [[CrossRef](#)]
22. Jaju, P.P.; Jaju, S.P. Cone-beam computed tomography: Time to move from ALARA to ALADA. *Imaging Sci. Dent.* **2015**, *45*, 263–265. [[CrossRef](#)] [[PubMed](#)]
23. Oenning, A.C.; Jacobs, R.; Salmon, B. ALADAIP, beyond ALARA and towards personalized optimization for paediatric cone-beam CT. *Int. J. Paediatr. Dent.* **2021**, *31*, 676–678. [[CrossRef](#)] [[PubMed](#)]
24. Hung, K.F.; Hui, L.; Yeung, A.W.K.; Jacobs, R.; Leung, Y.Y.; Bornstein, M.M. An analysis of patient dose received during cone-beam computed tomography in relation to scan settings and imaging indications as seen in a dental institution in order to establish institutional diagnostic reference levels. *Dentomaxillofac. Radiol.* **2022**, *51*, 20200529. [[CrossRef](#)] [[PubMed](#)]
25. Yeung, A.W.K.; Wong, N.S.M. Reject Rates of Radiographic Images in Dentomaxillofacial Radiology: A Literature Review. *Int. J. Environ. Res. Public Health* **2021**, *18*, 8076. [[CrossRef](#)]
26. Hung, K.; Hui, L.; Yeung, A.W.K.; Scarfe, W.C.; Bornstein, M.M. Image retake rates of cone beam computed tomography in a dental institution. *Clin. Oral Investig.* **2020**, *24*, 4501–4510. [[CrossRef](#)]
27. Beale, T.J.; Madani, G.; Morley, S.J. Imaging of the paranasal sinuses and nasal cavity: Normal anatomy and clinically relevant anatomical variants. *Semin. Ultrasound CT MRI* **2009**, *30*, 2–16. [[CrossRef](#)]
28. Rege, I.C.C.; Sousa, T.O.; Leles, C.R.; Mendonça, E.F. Occurrence of maxillary sinus abnormalities detected by cone beam CT in asymptomatic patients. *BMC Oral Health* **2012**, *12*, 30. [[CrossRef](#)]
29. Ella, B.; Sédarat, C.; Da Costa Noble, R.; Normand, E.; Lauverjat, Y.; Siberchicot, F.; Caix, P.; Zwetyenga, N. Vascular connections of the lateral wall of the sinus: Surgical effect in sinus augmentation. *Int. J. Oral Maxillofac. Implant.* **2008**, *23*, 1047–1052.
30. Jensen, S.S.; Eriksen, J.; Schiodt, M. Severe bleeding after sinus floor elevation using the transcrestal technique: A case report. *Eur. J. Oral Implant.* **2012**, *5*, 287–291.
31. Ilgüy, D.; Ilgüy, M.; Dolekoglu, S.; Fisekcioglu, E. Evaluation of the posterior superior alveolar artery and the maxillary sinus with CBCT. *Braz. Oral Res.* **2013**, *27*, 431–437. [[CrossRef](#)] [[PubMed](#)]
32. Tehranchi, M.; Taleghani, F.; Shahab, S.; Nouri, A. Prevalence and location of the posterior superior alveolar artery using cone-beam computed tomography. *Imaging Sci. Dent.* **2017**, *47*, 39–44. [[CrossRef](#)] [[PubMed](#)]

33. Danesh-Sani, S.A.; Movahed, A.; ElChaar, E.S.; Chong Chan, K.; Amintavakoli, N. Radiographic evaluation of maxillary sinus lateral wall and posterior superior alveolar artery anatomy: A cone-beam computed tomographic study. *Clin. Implant Dent. Relat. Res.* **2017**, *19*, 151–160. [[CrossRef](#)]
34. Jung, J.; Yim, J.-H.; Kwon, Y.-D.; Al-Nawas, B.; Kim, G.-T.; Choi, B.-J.; Lee, D.-W. A radiographic study of the position and prevalence of the maxillary arterial endosseous anastomosis using cone beam computed tomography. *Int. J. Oral Maxillofac. Implant.* **2011**, *26*, 1273–1278.
35. Lozano-Carrascal, N.; Salomó-Coll, O.; Gehrke, S.A.; Calvo-Guirado, J.L.; Hernández-Alfaro, F.; Gargallo-Albiol, J. Radiological evaluation of maxillary sinus anatomy: A cross-sectional study of 300 patients. *Ann. Anat. -Anat. Anz.* **2017**, *214*, 1–8. [[CrossRef](#)]
36. Ang, K.-Y.; Ang, K.-L.; Ngeow, W.C. The prevalence and location of the posterior superior alveolar artery in the maxillary sinus wall: A preliminary computed-cone beam study. *Saudi Dent. J.* **2022**, *34*, 629–635. [[CrossRef](#)] [[PubMed](#)]
37. Varela-Centelles, P.; Loira-Gago, M.; Seoane-Romero, J.; Takkouche, B.; Monteiro, L.; Seoane, J. Detection of the posterior superior alveolar artery in the lateral sinus wall using computed tomography / cone beam computed tomography: A prevalence meta-analysis study and systematic review. *Int. J. Oral Maxillofac. Surg.* **2015**, *44*, 1405–1410. [[CrossRef](#)]
38. Basma, H.; Saleh, I.; Abou-Arraj, R.; Li, P.; Benavides, E.; Wang, H.-L.; Chang, H.-L. Association between lateral wall thickness and sinus membrane perforation during lateral sinus elevation: A retrospective study. *Int. J. Oral Implant* **2021**, *14*, 77–85.
39. Kiakojori, A.; Nasab, S.P.M.; Abesi, F.; Gholinia, H. Radiographic assessment of maxillary sinus lateral wall thickness in edentulous posterior maxilla. *Electron. Physician* **2017**, *9*, 5948–5953. [[CrossRef](#)]
40. Lim, E.L.; Ngeow, W.C.; Lim, D. The implications of different lateral wall thicknesses on surgical access to the maxillary sinus. *Braz. Oral Res.* **2017**, *31*, e97. [[CrossRef](#)]
41. Rahpeyma, A.; Khajehahmadi, S.; Amini, P. Alveolar antral artery: Does its diameter correlate with maxillary lateral wall thickness in dentate patients? *Iran. J. Otorhinolaryngol.* **2014**, *26*, 163–167. [[PubMed](#)]
42. Pelinsari Lana, J.; Moura Rodrigues Carneiro, P.; de Carvalho Machado, V.; Eduardo Alencar de Souza, P.; Ricardo Manzi, F.; Campolina Rebello Horta, M. Anatomic variations and lesions of the maxillary sinus detected in cone beam computed tomography for dental implants. *Clin. Oral Implant. Res.* **2012**, *23*, 1398–1403. [[CrossRef](#)]
43. Cavalcanti, M.C.; Guirado, T.E.; Sapata, V.M.; Costa, C.; Pannuti, C.M.; Jung, R.E.; César Neto, J.B. Maxillary sinus floor pneumatization and alveolar ridge resorption after tooth loss: A cross-sectional study. *Braz. Oral Res.* **2018**, *32*, e64. [[CrossRef](#)] [[PubMed](#)]
44. Wu, X.; Cai, Q.; Huang, D.; Xiong, P.; Shi, L. Cone-beam computed tomography-based analysis of maxillary sinus pneumatization extended into the alveolar process in different age groups. *BMC Oral Health* **2022**, *22*, 393. [[CrossRef](#)]
45. Hamdy, R.M. Three-dimensional linear and volumetric analysis of maxillary sinus pneumatization. *J. Adv. Res.* **2014**, *5*, 387–395. [[CrossRef](#)]
46. Lombardi, T.; Bernardello, F.; Berton, F.; Porrelli, D.; Rapani, A.; Camurri Piloni, A.; Fiorillo, L.; Di Lenarda, R.; Stacchi, C. Efficacy of alveolar ridge preservation after maxillary molar extraction in reducing crestal bone resorption and sinus pneumatization: A multicenter prospective case-control study. *BioMed Res. Int.* **2018**, *2018*, 9352130. [[CrossRef](#)] [[PubMed](#)]
47. Günaçar, D.N.; Köse, T.E.; Arsan, B.; Aydın, E.Z. Radioanatomic study of maxillary sinus palatal process pneumatization. *Oral Radiol.* **2022**, *38*, 398–404. [[CrossRef](#)]
48. Alsufyani, N.; El-Hakim, H.; Major, P. Prevalence of maxillary sinus hypoplasia and association with variations in the sinonasal complex: A cone beam CT study. *Clin. Oral Investig.* **2021**, *25*, 5463–5471. [[CrossRef](#)]
49. Allareddy, V.; Vincent, S.D.; Hellstein, J.W.; Qian, F.; Smoker, W.R.; Ruprecht, A. Incidental findings on cone beam computed tomography images. *Int. J. Dent.* **2012**, *2012*, 871532. [[CrossRef](#)]
50. Jafari-Pozve, N.; Sheikhi, M.; Ataie-Khorasgani, M.; Jafari-Pozve, S. Aplasia and hypoplasia of the maxillary sinus: A case series. *Dent. Res. J.* **2014**, *11*, 615–617.
51. Alsufyani, N.A.; Major, M.P.; Major, P.W. Relationship between maxillary sinus hypoplasia and maxillary occlusal cant: A cone beam CT study. *BioMed Res. Int.* **2021**, *2022*, 4651514. [[CrossRef](#)]
52. Klijn, R.; Van Den Beucken, J.; Bronkhorst, E.; Berge, S.; Meijer, G.; Jansen, J. Predictive value of ridge dimensions on autologous bone graft resorption in staged maxillary sinus augmentation surgery using Cone-Beam CT. *Clin. Oral Implant. Res.* **2012**, *23*, 409–415. [[CrossRef](#)] [[PubMed](#)]
53. Okada, T.; Kanai, T.; Tachikawa, N.; Munakata, M.; Kasugai, S. Long-term radiographic assessment of maxillary sinus floor augmentation using beta-tricalcium phosphate: Analysis by cone-beam computed tomography. *Int. J. Implant Dent.* **2016**, *2*, 8. [[CrossRef](#)] [[PubMed](#)]
54. Kivovics, M.; Szabó, B.T.; Németh, O.; Iványi, D.; Trimmel, B.; Szmirmova, I.; Orhan, K.; Mijiritsky, E.; Szabó, G.; Dobó-Nagy, C. Comparison between micro-computed tomography and cone-beam computed tomography in the assessment of bone quality and a long-term volumetric study of the augmented sinus grafted with an albumin impregnated allograft. *J. Clin. Med.* **2020**, *9*, 303. [[CrossRef](#)] [[PubMed](#)]
55. Kwon, J.J.; Hwang, J.; Kim, Y.D.; Shin, S.H.; Cho, B.H.; Lee, J.Y. Automatic three-dimensional analysis of bone volume and quality change after maxillary sinus augmentation. *Clin. Implant Dent. Relat. Res.* **2019**, *21*, 1148–1155. [[CrossRef](#)] [[PubMed](#)]
56. Soardi, C.M.; Zaffe, D.; Motroni, A.; Wang, H.L. Quantitative comparison of cone beam computed tomography and microradiography in the evaluation of bone density after maxillary sinus augmentation: A preliminary study. *Clin. Implant Dent. Relat. Res.* **2014**, *16*, 557–564. [[CrossRef](#)]

57. Bornstein, M.M.; Seiffert, C.; Maestre-Ferrín, L.; Fodich, I.; Jacobs, R.; Buser, D.; von Arx, T. An Analysis of Frequency, Morphology, and Locations of Maxillary Sinus Septa Using Cone Beam Computed Tomography. *Int. J. Oral Maxillofac. Implant.* **2016**, *31*, 280–287. [[CrossRef](#)]
58. Tadinada, A.; Jalali, E.; Al-Salman, W.; Jambhekar, S.; Katechia, B.; Almas, K. Prevalence of bony septa, antral pathology, and dimensions of the maxillary sinus from a sinus augmentation perspective: A retrospective cone-beam computed tomography study. *Imaging Sci. Dent.* **2016**, *46*, 109–115. [[CrossRef](#)]
59. Hungerbühler, A.; Rostetter, C.; Lübbers, H.-T.; Rucker, M.; Stadlinger, B. Anatomical characteristics of maxillary sinus septa visualized by cone beam computed tomography. *Int. J. Oral Maxillofac. Surg.* **2019**, *48*, 382–387. [[CrossRef](#)]
60. Orhan, K.; Seker, B.K.; Aksoy, S.; Bayindir, H.; Berberoğlu, A.; Seker, E. Cone beam CT evaluation of maxillary sinus septa prevalence, height, location and morphology in children and an adult population. *Med. Princ. Pract.* **2013**, *22*, 47–53. [[CrossRef](#)]
61. Sigaroudi, A.K.; Kajan, Z.D.; Rastgar, S.; Asli, H.N. Frequency of different maxillary sinus septal patterns found on cone-beam computed tomography and predicting the associated risk of sinus membrane perforation during sinus lifting. *Imaging Sci. Dent.* **2017**, *47*, 261–267. [[CrossRef](#)] [[PubMed](#)]
62. Shanbhag, S.; Karnik, P.; Shirke, P.; Shanbhag, V. Cone-beam computed tomographic analysis of sinus membrane thickness, ostium patency, and residual ridge heights in the posterior maxilla: Implications for sinus floor elevation. *Clin. Oral Implant. Res.* **2014**, *25*, 755–760. [[CrossRef](#)] [[PubMed](#)]
63. Guo, Z.Z.; Liu, Y.; Qin, L.; Song, Y.L.; Xie, C.; Li, D.H. Longitudinal response of membrane thickness and ostium patency following sinus floor elevation: A prospective cohort study. *Clin. Oral Implant. Res.* **2016**, *27*, 724–729. [[CrossRef](#)] [[PubMed](#)]
64. Yeung, A.W.K.; Colsohl, N.; Montalvao, C.; Hung, K.; Jacobs, R.; Bornstein, M.M. Visibility, location, and morphology of the primary maxillary sinus ostium and presence of accessory ostia: A retrospective analysis using cone beam computed tomography (CBCT). *Clin. Oral Investig.* **2019**, *23*, 3977–3986. [[CrossRef](#)] [[PubMed](#)]
65. Hung, K.; Montalvao, C.; Yeung, A.W.K.; Li, G.; Bornstein, M.M. Frequency, location, and morphology of accessory maxillary sinus ostia: A retrospective study using cone beam computed tomography (CBCT). *Surg. Radiol. Anat.* **2020**, *42*, 219–228. [[CrossRef](#)]
66. Ali, I.K.; Sansare, K.; Karjodkar, F.R.; Vanga, K.; Salve, P.; Pawar, A.M. Cone-beam computed tomography analysis of accessory maxillary ostium and Haller cells: Prevalence and clinical significance. *Imaging Sci. Dent.* **2017**, *47*, 33–37. [[CrossRef](#)]
67. Shetty, S.; Al Bayatti, S.W.; Al-Rawi, N.H.; Samsudin, R.; Marei, H.; Shetty, R.; Abdelmagyd, H.A.; Reddy, S. A study on the association between accessory maxillary ostium and maxillary sinus mucosal thickening using cone beam computed tomography. *Head Face Med.* **2021**, *17*, 28. [[CrossRef](#)]
68. Lu, Y.; Liu, Z.; Zhang, L.; Zhou, X.; Zheng, Q.; Duan, X.; Zheng, G.; Wang, H.; Huang, D. Associations between maxillary sinus mucosal thickening and apical periodontitis using cone-beam computed tomography scanning: A retrospective study. *J. Endod.* **2012**, *38*, 1069–1074. [[CrossRef](#)]
69. Aksoy, U.; Orhan, K. Association between odontogenic conditions and maxillary sinus mucosal thickening: A retrospective CBCT study. *Clin. Oral Investig.* **2019**, *23*, 123–131. [[CrossRef](#)] [[PubMed](#)]
70. Bornstein, M.M.; Wasmer, J.; Sendi, P.; Janner, S.F.; Buser, D.; Von Arx, T. Characteristics and dimensions of the Schneiderian membrane and apical bone in maxillary molars referred for apical surgery: A comparative radiographic analysis using limited cone beam computed tomography. *J. Endod.* **2012**, *38*, 51–57. [[CrossRef](#)] [[PubMed](#)]
71. Nascimento, E.H.L.; Pontual, M.L.A.; Pontual, A.A.; Freitas, D.Q.; Perez, D.E.C.; Ramos-Perez, F.M. Association between odontogenic conditions and maxillary sinus disease: A study using cone-beam computed tomography. *J. Endod.* **2016**, *42*, 1509–1515. [[CrossRef](#)] [[PubMed](#)]
72. Ren, S.; Zhao, H.; Liu, J.; Wang, Q.; Pan, Y. Significance of maxillary sinus mucosal thickening in patients with periodontal disease. *Int. Dent. J.* **2015**, *65*, 303–310. [[CrossRef](#)]
73. Cao, Z.; Yuan, J. Changes in Maxillary Sinus Mucosal Thickening following the Extraction of Teeth with Advanced Periodontal Disease: A Retrospective Study Using Cone-Beam Computed Tomography. *BioMed Res. Int.* **2021**, *2021*, 6688634. [[CrossRef](#)] [[PubMed](#)]
74. Eggmann, F.; Connert, T.; Bühler, J.; Dagassan-Berndt, D.; Weiger, R.; Walter, C. Do periapical and periodontal pathologies affect Schneiderian membrane appearance? Systematic review of studies using cone-beam computed tomography. *Clin. Oral Investig.* **2017**, *21*, 1611–1630. [[CrossRef](#)] [[PubMed](#)]
75. Yeung, A.W.K.; Tanaka, R.; Khong, P.-L.; von Arx, T.; Bornstein, M.M. Frequency, location, and association with dental pathology of mucous retention cysts in the maxillary sinus. A radiographic study using cone beam computed tomography (CBCT). *Clin. Oral Investig.* **2018**, *22*, 1175–1183. [[CrossRef](#)] [[PubMed](#)]
76. Hung, K.; Hui, L.; Yeung, A.W.K.; Wu, Y.; Hsung, R.T.-C.; Bornstein, M.M. Volumetric analysis of mucous retention cysts in the maxillary sinus: A retrospective study using cone-beam computed tomography. *Imaging Sci. Dent.* **2021**, *51*, 117–127. [[CrossRef](#)]
77. Ren, L.; Chen, C.; Li, N.; Hu, J.; Jiang, Z.; Yang, G. Prevalence of and factors associated with maxillary sinus cyst in a Chinese population. *J. Oral Sci.* **2022**, *64*, 22–27. [[CrossRef](#)] [[PubMed](#)]
78. Cho, B.-H.; Jung, Y.-H.; Hwang, J.-J. Maxillary antroliths detected by cone-beam computed tomography in an adult dental population. *Imaging Sci. Dent.* **2019**, *49*, 59–63. [[CrossRef](#)]

79. Chen, H.-H.; Yi, C.-A.; Chen, Y.-C.; Huang, H.-H. Anatomical characteristics of maxillary sinus antroliths and their influence on sinus membrane thickness: A retrospective cone beam computed tomography analysis. *Int. J. Oral Maxillofac. Surg.* **2021**, *50*, 1107–1112. [[CrossRef](#)]
80. Kawai, T.; Tanaka, R.; Yeung, A.W.K.; von Arx, T.; Bornstein, M.M. Frequency and type of incidentally detected radiodensities in the maxillary sinus: A retrospective analysis using cone beam computed tomography (CBCT). *Clin. Oral Investig.* **2019**, *23*, 1091–1099. [[CrossRef](#)]
81. Chen, H.H.; Yi, C.A.; Chen, Y.C.; Tsai, C.C.; Lin, P.Y.; Huang, H.H. Influence of maxillary antrolith on the clinical outcome of implants placed simultaneously with osteotome sinus floor elevation: A retrospective radiographic study. *Clin. Implant Dent. Relat. Res.* **2021**, *23*, 833–841. [[CrossRef](#)] [[PubMed](#)]
82. Tilaveridis, I.; Stefanidou, A.; Kyrgidis, A.; Tilaveridis, S.; Tilaveridou, S.; Zouloumis, L. Foreign Bodies of Dental Iatrogenic Origin Displaced in the Maxillary Sinus—A Safety and Efficacy Analysis of a Retrospective Study. *Ann. Maxillofac. Surg.* **2022**, *12*, 33–38. [[PubMed](#)]
83. Rahnama, M.; Łobacz, M.; Kielbowicz, D.; Graszka, J. Foreign body in the maxillary sinus—a case report. *Curr. Issues Pharm. Med. Sci.* **2012**, *25*, 15–17. [[CrossRef](#)]
84. Sgaramella, N.; Tartaro, G.; D’Amato, S.; Santagata, M.; Colella, G. Displacement of dental implants into the maxillary sinus: A retrospective study of twenty-one patients. *Clin. Implant Dent. Relat. Res.* **2016**, *18*, 62–72. [[CrossRef](#)] [[PubMed](#)]
85. Shao, L.; Qin, X.; Ma, Y. Removal of maxillary sinus metallic foreign body like a hand sewing needle by magnetic iron. *Int. J. Clin. Pediatric Dent.* **2014**, *7*, 61–64. [[CrossRef](#)]
86. Motoyoshi, M.; Sanuki-Suzuki, R.; Uchida, Y.; Saiki, A.; Shimizu, N. Maxillary sinus perforation by orthodontic anchor screws. *J. Oral Sci.* **2015**, *57*, 95–100. [[CrossRef](#)]
87. Patil, S.; Albogami, S.; Hosmani, J.; Mujoo, S.; Kamil, M.A.; Mansour, M.A.; Abdul, H.N.; Bhandi, S.; Ahmed, S.S. Artificial Intelligence in the Diagnosis of Oral Diseases: Applications and Pitfalls. *Diagnostics* **2022**, *12*, 1029. [[CrossRef](#)]
88. Jung, S.-K.; Lim, H.-K.; Lee, S.; Cho, Y.; Song, I.-S. Deep active learning for automatic segmentation of maxillary sinus lesions using a convolutional neural network. *Diagnostics* **2021**, *11*, 688. [[CrossRef](#)]
89. Morgan, N.; Van Gerven, A.; Smolders, A.; de Faria Vasconcelos, K.; Willems, H.; Jacobs, R. Convolutional neural network for automatic maxillary sinus segmentation on cone-beam computed tomographic images. *Sci. Rep.* **2022**, *12*, 7523. [[CrossRef](#)]
90. Hung, K.F.; Ai, Q.Y.H.; King, A.D.; Bornstein, M.M.; Wong, L.M.; Leung, Y.Y. Automatic detection and segmentation of morphological changes of the maxillary sinus mucosa on cone-beam computed tomography images using a three-dimensional convolutional neural network. *Clin. Oral Investig.* **2022**, *26*, 3987–3998. [[CrossRef](#)]
91. Choi, H.; Jeon, K.J.; Kim, Y.H.; Ha, E.-G.; Lee, C.; Han, S.-S. Deep learning-based fully automatic segmentation of the maxillary sinus on cone-beam computed tomographic images. *Sci. Rep.* **2022**, *12*, 14009. [[CrossRef](#)] [[PubMed](#)]
92. Serindere, G.; Bilgili, E.; Yesil, C.; Ozveren, N. Evaluation of maxillary sinusitis from panoramic radiographs and cone-beam computed tomographic images using a convolutional neural network. *Imaging Sci. Dent.* **2022**, *52*, 187–195. [[CrossRef](#)] [[PubMed](#)]
93. Kurt Bayrakdar, S.; Orhan, K.; Bayrakdar, I.S.; Bilgir, E.; Ezhov, M.; Gusarev, M.; Shumilov, E. A deep learning approach for dental implant planning in cone-beam computed tomography images. *BMC Med. Imaging* **2021**, *21*, 86. [[CrossRef](#)] [[PubMed](#)]
94. Al-Amodi, A.; Kamel, I.; Al-Rawi, N.H.; Uthman, A.; Shetty, S. Accuracy of Linear Measurements of Maxillary Sinus Dimensions in Gender Identification Using Machine Learning. In Proceedings of the 2021 14th International Conference on Developments in eSystems Engineering (DeSE), Sharjah, United Arab Emirates, 7–10 December 2021; pp. 407–412.
95. Saric, R.; Kevric, J.; Hadziabdic, N.; Osmanovic, A.; Kadic, M.; Saracevic, M.; Jokic, D.; Rajs, V. Dental age assessment based on CBCT images using machine learning algorithms. *Forensic Sci. Int.* **2022**, *334*, 111245. [[CrossRef](#)]
96. Estrela, C.R.; Bueno, M.R.; Estrela, M.R.; Estrela, L.R.; Guedes, O.A.; Azevedo, B.C.; Cintra, L.T.A.; Estrela, C. Frequency and risk factors of maxillary sinusitis of endodontic origin evaluated by a dynamic navigation and a new filter of cone-beam computed tomography. *J. Endod.* **2022**, *48*, 1263–1272. [[CrossRef](#)]